Hindawi
Geofluids
Volume 2022, Article ID 1471264, 12 pages
https://doi.org/10.1155/2022/1471264

Research Article

Experiment Analysis of Drilling Feedback Signal from Simulation of Roadway Roof

Gang Guo,[1] **Haoyuan Zhao**,[2] **Zhilong Qi**,[2] **Chenjun Hu**,[3] **Baofu Zhao**,[3] **and Shengzhi Wang**[3]

[1]*China Coal Energy Group Co., Ltd., Beijing 100120, China*
[2]*China Coal Shaanxi Yulin Chemical Energy Co., Ltd., Yulin Shaanxi 719054, China*
[3]*China Coal (Tianjin) Underground Engineering Intelligent Research Institute Co., Ltd., Tianjin 300121, China*

Correspondence should be addressed to Gang Guo; guogang0124@163.com

Received 8 August 2022; Revised 15 September 2022; Accepted 27 September 2022; Published 12 October 2022

Academic Editor: Liang Xin

To simulate the condition of unstable rock formation in the stable rock formation of the roadway roof, the complete and broken rock formations on the roadway roof were simulated by superimposing and combining complete specimens and broken specimens, hence providing an appropriate way to obtain the drilling vibration signals to find regular patterns which can be used to judge the state of the rock layers. The Fourier transform analysis method and the wavelet transform analysis method are, respectively, used for the vibration signals to extract the eigenvalues of the vibration signals that are quite different in the complete layer and broken layers. Effective values, kurtosis factor, pulse factors, and gravity amplitude were used to construct the eigenvectors, which were most suitable as the basis for judging the integrity of rock formation after analysis, providing an effective way to deal with drilling signal. The wavelet threshold denoising could adaptively reduce the noise of the signals, and the unbiased likelihood estimation threshold rule had the best denoising effect. Well, through the extraction and comparison of the wavelet feature-scale entropy values, it is concluded that the wavelet analysis can be used as a reference rather than a decisive factor to determine the complete and broken layers. And more research is needed to determine the selection method of wavelet.

1. Introduction

The research of drilling signal of anchor hole is mainly to judge the rock properties of drilling position by the thrust torque, drilling rate, rotational speed, and other parameters of the drill bit [1–3]. In recent years, the variation and relationship of drilling vibration signals in different rock strata have been studied. The state of rock strata can be judged by vibration signals [4, 5]. However, in the research of identifying roof strata by vibration signals, insufficient data volume, low recognition accuracy, and the need for manual processing of vibration signals are all factors that restrict the identification of roof lithology by vibration signals [6–8]. Therefore, this study takes the analysis algorithm of vibration signals as the core and generates the corresponding computer program, so that the input vibration signals can be automatically converted into information about the rock strata. If it can be used in engineering practice, the information of roof strata can be obtained in real time when driving, the supporting parameters can be changed in time, the support cost can be saved, and the risk of roof accidents can be greatly reduced [9, 10].

The research on the formation condition judged by vibration signals has been relatively mature in the field of oil drilling. Andrzej et al. and Li et al. [11, 12] studied the relationship between drilling signals and rock properties in the process of drilling through the method of similar simulation and came to the conclusion that the drilling speed and rotational speed generally had a negative exponential relationship with the rock mass's Protodyakonov number, which could be used to identify the roof rock properties. Xue et al. [13, 14] stablished an elastic damage constitutive

Figure 1: Complete layer specimen.

Figure 2: Broken layer specimen.

model and revealed the changes in microstructure and mechanical properties of low-permeability coal under fatigue fracturing tests. Yan et al. and Kang et al. [15, 16] found that rock vibration information could reflect rock properties more accurately than acoustic information, and the change of axial drilling pressure would not significantly change the acoustic and vibration spectrum characteristics. Krishnan and Anne and Wang et al. [17, 18] introduced the Harol transform method and fast algorithm and compared with Fourier transform; it is pointed out that the Harol transform has a better effect on mechanical vibration signal analysis.

The existing research on the use of drilling information has been carried out, showing that the nature of coal rock will affect the drilling signal, which has a practical role in practical engineering [19–22]. Some scholars decompose and transform drilling signals and use different methods to analyze and process them, finding some practical rules of drilling signal processing [23–26]. The current research method can judge the formation information and drilling tool working state by drilling string vibration signals, but there are still some problems when judging roof information by drilling vibration signals in roadway. The vibration signals obtained have less effective information, more noise, and poor denoising ability, requiring manual analysis and identification [27–31]. Therefore, improving the signal-to-noise ratio to maximize the retention of useful information after denoising and processing a large amount of vibration signals automatically to judge the integrity of rock strata quickly and accurately are two technical challenges that need to be overcome.

2. Test Method

2.1. Test Specimens and Equipment. Ordinary Portland cement is used as the main material, and a certain amount of medium sand, stone, coal, and other materials with a diameter of less than 25 mm is added [32, 33]. After mixing by a mixer, these materials can be used to simulate the roof strata of a roadway. The materials are mixed thoroughly and placed in a prepared mold with dimensions of 750 mm × 400 mm × 100 mm. After the mixture is completely dried, a complete layer specimen used to simulate a complete roof stratum is ready (Figure 1). Some of the complete layer specimens expected to be broken layer specimens are damaged by the text frames, resulting in some roughly uniform cracks in their surface (Figure 2).

As shown in Figure 3, the specimens are combined in the order of "complete layer-broken layer-complete layer-broken layer-complete layer" to simulate the conditions where unstable rock strata are in the stable rock strata of the roadway roof. These layers are named as "complete layer 1," "broken layer 1," "complete layer 2," "broken layer 2," and "complete layer 3," respectively, from bottom to top, and fixed with steel plates as drilling test specimens.

According to the knowledge of elastic-plastic mechanics, the distance between two boreholes that do not affect each other is 20d (d is the diameter of the borehole) in a homogeneous medium. A 28 mm drill bit was designed for this drilling test, so the minimum distance between the two boreholes is 125.22 mm. Boreholes were arranged according to Figure 4. The minimum distance between the two boreholes was 152 mm, and between the borehole and the edge of the specimen was 136 mm, which could meet the requirements of drilling spacing.

ULT2756 DC response acceleration sensor is used to test the vibration signal because of its advantages such as low zero drift, low noise, and strong anti-interference capability. The sensor measures the acceleration of the drill pipe as vibration information. And a data acquisition module with 37.9 Hz acquisition frequency collects acceleration data per unit time. The power supply uses a 3.7 V, 2000 mAh rechargeable battery to power the sensor and the data acquisition module. The position of the drill bit in the combined specimens is recorded so that the vibration signals from complete and broken layers can be distinguished.

2.2. Test Design Method. To study the relationship between drilling vibration signal and rock integrity, the vibration signals and the displacement of the drill bit, which helps distinguish signals from different layers, should be collected and recorded in real time. The collected signals should be analyzed by a variety of analysis methods. And their eigenvalues should be calculated to establish a relationship with the integrity of the specimens that allows judging the integrity of real roofs.

To make the vibration signals represent the real vibration states of the drill pipe more accurately while ensuring the authenticity and accessibility of the drilling operation, the vibration acceleration sensor was installed at the joint between the bottom of the drill pipe and the rig with a

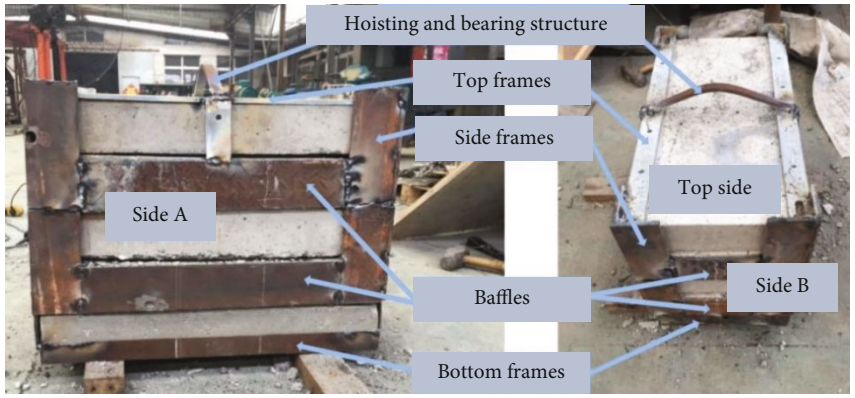

Figure 3: Combined specimens.

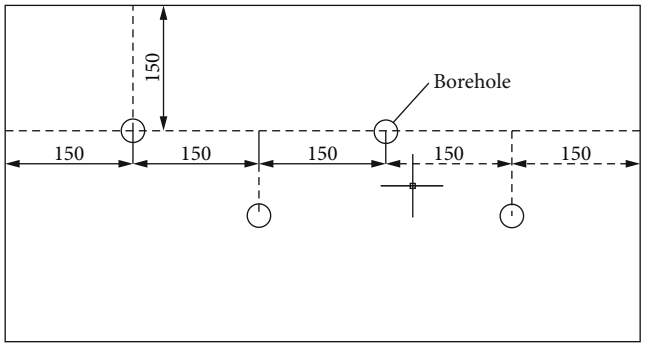

Figure 4: Drilling layout.

special connecting rod. At the same time, the centers of these parts were aligned, which allowed for the accurate collection of vibration information without disrupting normal drilling operations.

Before the test, each test instrument was debugged, so that it was in a stable working state. The vibration signal and displacement started to be recorded when the drill bit contacted with the bottom surface of specimens. The drill pipe was always perpendicular to the ground during drilling.

3. Time and Frequency Domain Analysis of Vibration Signal Based on Fourier Transform

3.1. Time and Frequency Domain Analysis Method. Time domain describes the relationship between the signal and time, and a time domain diagram of signal changing with time is obtained by taking time as an abscissa and the physical signal as an ordinate. Time domain eigenvalues can be divided into two categories, namely, dimensional eigenvalues and dimensionless eigenvalues. Dimensional eigenvalues include peak value, mean value, mean amplitude, and mean square value. However, they are not conducive to practical application because they are affected by external conditions. Therefore, some dimensionless physical quantities are often used, such as peak factor, kurtosis factor, and pulse factor. They are not affected by experimental conditions, making it easier to find regular patterns.

Mean amplitude of vibration is obtained by calculating the mean value of the absolute values of the signal data. The expression is shown in

$$\bar{x}_p = \frac{\sum_{i=1}^{n} X_i}{N}. \tag{1}$$

Effective value, also called root mean square, is calculated by averaging the squares of signal data and then finding the arithmetic square root, which can also represent the energy of signals. The expression is as follows:

$$X_{\text{rms}} = \sqrt{\frac{\sum_{i=1}^{n} X_i}{N}} = \frac{\sqrt{X_1{}^2 + X_2{}^2 + \cdots\cdots + X_N{}^2}}{N}. \tag{2}$$

Kurtosis factor, a normalized fourth-order central moment of signal data, is a response to the impact characteristics of vibration signals. The expression is as follows:

$$K_4 = \frac{E\left[(X-\mu)^4\right]}{\sigma^4}. \tag{3}$$

Pulse factor, which is a ratio of the peak value to the mean amplitude of signal data, can reflect the magnitude of the impact of signals. The expression is as follows:

$$P = \frac{X_{\text{peak}}}{\bar{x}_p} = X_{\text{peak}} \bullet \frac{N}{\sum_{i=1}^{n} X_i}. \tag{4}$$

Frequency domain is a coordinate system used to describe the frequency characteristics of signals. Frequency domain diagrams use frequencies as an abscissa, depicting the amplitude of signals at each frequency. The frequency domain representation can also include the phase shift information of each sine curve so that the frequency components can be recombined to recover the original time signal.

Fourier transform can transform the distribution of a signal in the time domain into that in the frequency domain. The formula is

$$F(\omega) = F[f(t)] = \int_{-\infty}^{+\infty} f(t) e^{-\text{iwt}} dt. \tag{5}$$

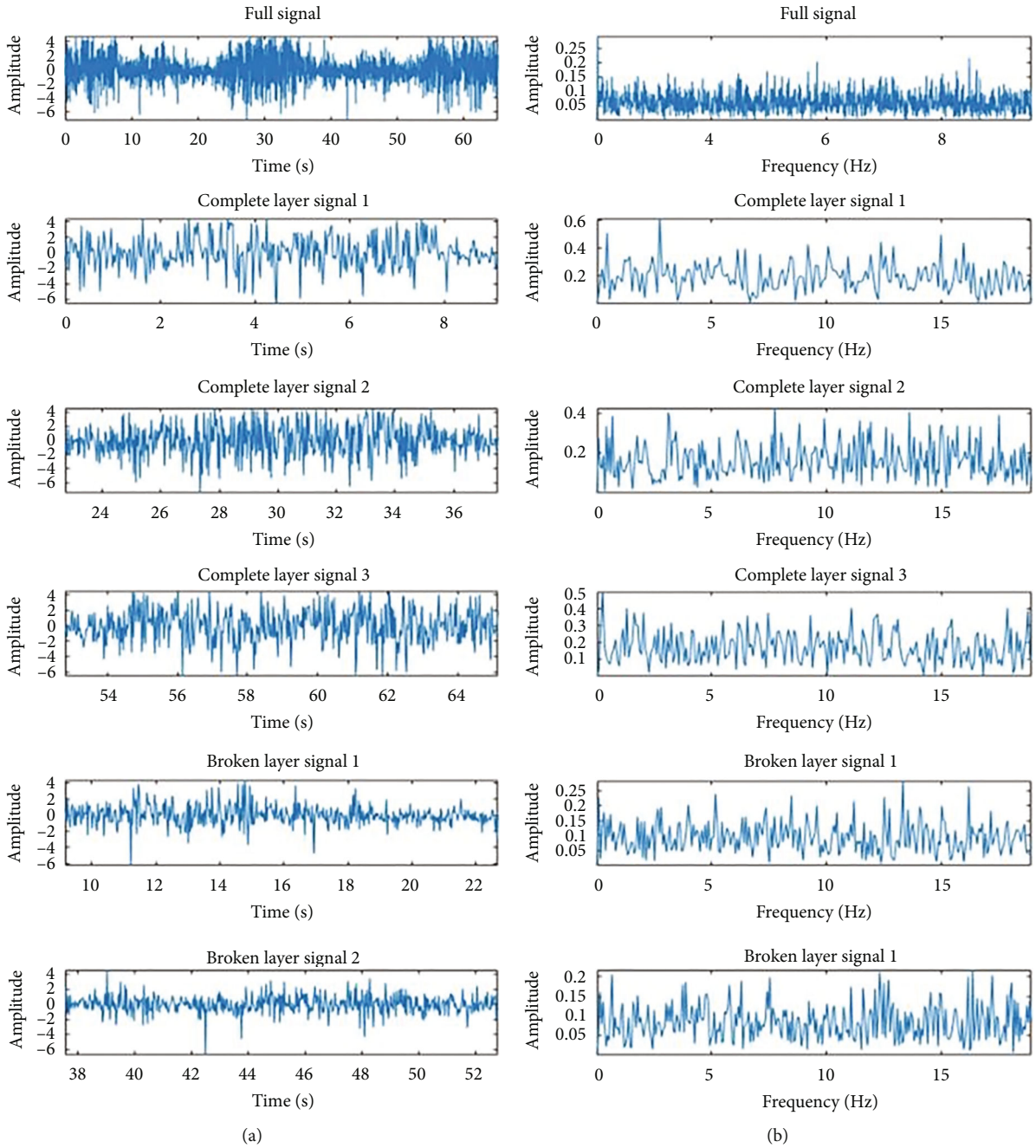

Figure 5: Time domain diagram (a) and frequency domain diagram (b) of the vibration signal from borehole 6.

The inverse Fourier transform can restore the distribution of a signal in frequency domain to the distribution of time domain. The formula is

$$F(\omega) = F^{-1}[f(\omega)] = \frac{1}{2\pi}\int_{-\infty}^{+\infty} f(\omega)e^{-\mathrm{iwt}}dt. \quad (6)$$

Fourier transform can transform a signal into the superposition of trigonometric functions, which has a good effect on the transformation of stationary signals. The vibration signal is a random signal, making it difficult to express its complete characteristics through the superposition of trigonometric functions. Therefore, it is not feasible to use Fourier transform directly, unless the signal data is processed by statistical analysis in advance.

Gravity frequency, the weight mean of signal data in the frequency range, is calculated by summing the products of each frequency and amplitude and then dividing the sum of the amplitudes. The calculation formula is as follows:

$$\mathrm{FC} = \frac{\sum_{i=1}^{n}\omega_i F(\omega_i)}{\sum_{i=1}^{N}\omega_i}. \quad (7)$$

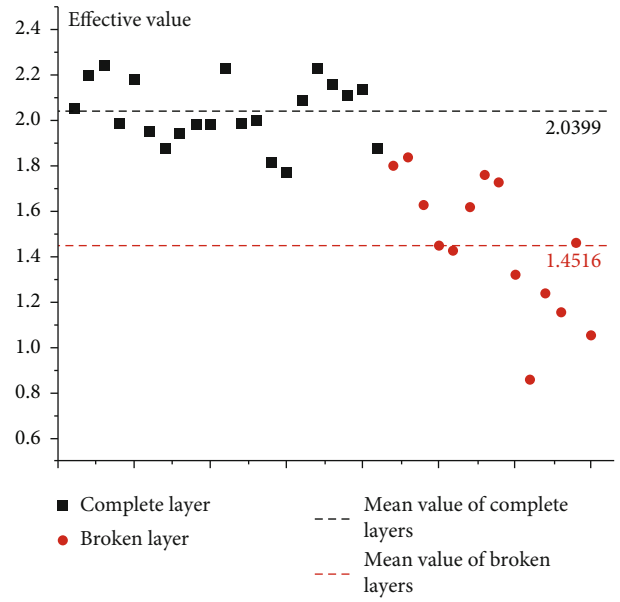

Figure 6: Effective value scatter diagram.

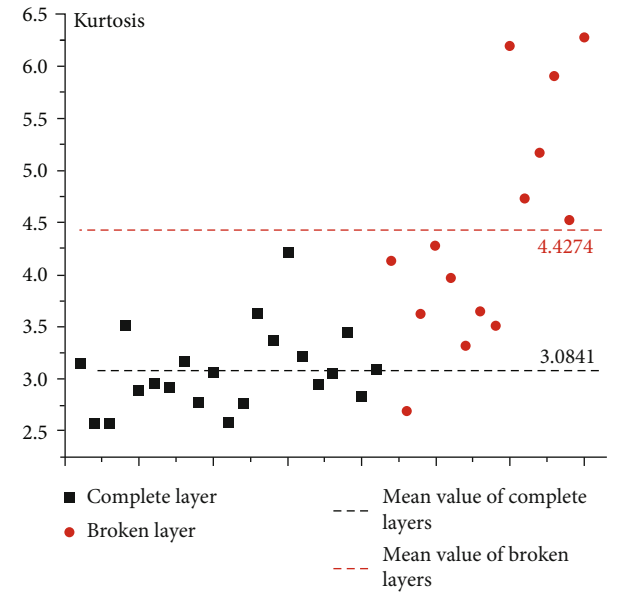

Figure 7: Kurtosis scatter diagram.

The definition of gravity amplitude is similar to that of gravity frequency. The calculation formula is

$$\mathrm{AC} = \frac{\sum_{i=1}^{n} \omega_i F(\omega_i)}{\sum_{i=1}^{N} F(\omega_i)}. \tag{8}$$

3.2. Analysis of Vibration Signal in Time Domain and Frequency Domain. The parts where the specimens had not been drilled into and had been drilled out of were removed from the full vibration signals that were obtained. And the remaining parts were divided into five sections according to the drilling displacement, which are recorded as complete layer signal 1, broken layer signal 1, complete layer signal 2, broken layer signal 2, and complete layer signal 3. The time domain diagram and frequency domain diagrams of the vibration signals were listed, so that the difference between the vibration signals from complete specimens and broken specimens could be observed clearly. The time domain and frequency domain diagrams of borehole 6 are shown here as an example (Figure 5).

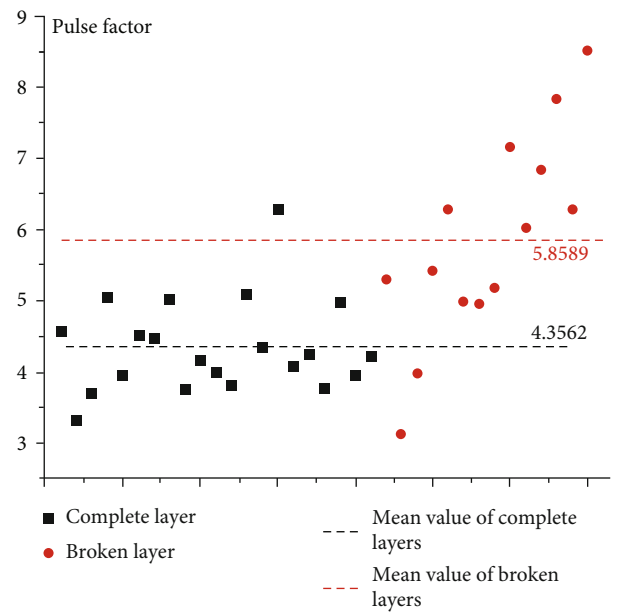

Figure 8: Pulse factor scatter diagram.

It can be seen from the time domain diagrams that, under the same condition of drilling pressure and rock properties, the amplitude of the vibration signals from complete layer is greater than that from broken layer. The reason for that was that the high hardness and strength of the complete layers created more resistance than broken layers on the drill bit when breaking them, resulting in stronger vibration. In other words, the broken layer specimens have been loose, making drilling easier. Moreover, there were more occasional sudden changes in the vibration signals from broken layers than those from the complete layers. That was caused by the small amount of large intact rock blocks in the broken layers. When drilling into the intact rock block, the drill bit was subjected to a sudden increase in resistance, reflected in the time domain diagram as a sudden change like a pulse signal.

By observing the frequency domain diagrams, the vibration signals are uniformly distributed in the whole frequency range, and the difference between the complete layer signals and the failure layer signals is not obvious in the peak frequency band. That may be due to the low sampling frequency of 37.9 Hz for the vibration signals, which fails to reflect the original frequency properties of them. The obvious differences between the complete layer signals and the broken layer signals in the frequency domain diagrams are the changes in frequency amplitude, which is significantly higher for the complete layers than for the broken layers.

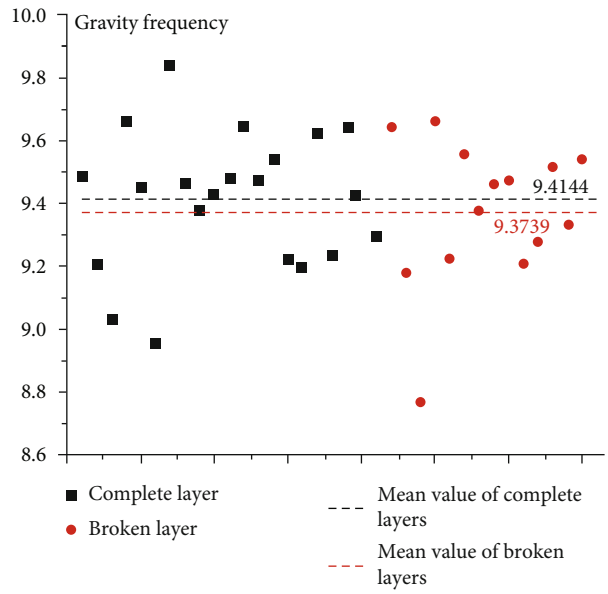

Figure 9: Gravity frequency scatter diagram.

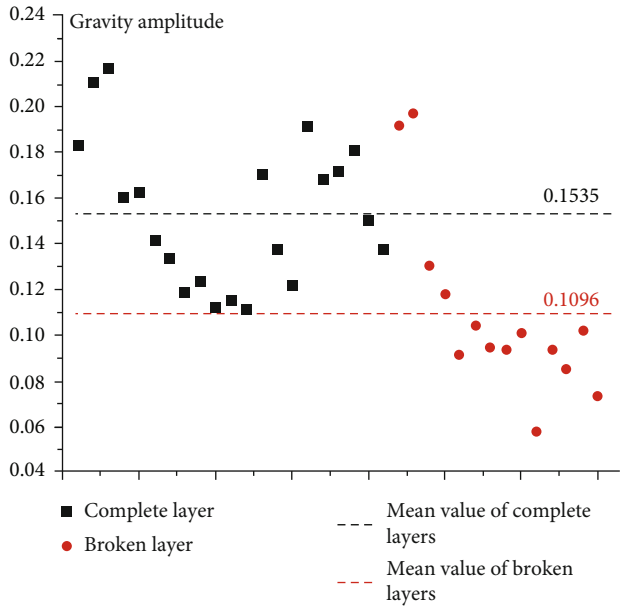

Figure 10: Gravity amplitude scatter diagram.

By comparing these signal data, it can be found that there are obvious differences in some eigenvalues between the complete layers and the broken layers, which can be used to determine whether the rock is broken. The eigenvalues are plotted as scatter plots to compare the differences between them clearly, as shown in Figures 6–10.

The scatter plots of the five eigenvalues from the vibration signal, effective value, kurtosis factor, pulse factor, gravity frequency, and gravity amplitude, are presented separately. In the effective value data, the mean value of the complete layers is 2.0399 with a variance of 0.0202, and the mean value of the broken layers is 1.4516 with a variance of 0.08881. In the kurtosis factor data, the mean value of the complete layers is 3.0841 with a variance of 0.1558, and the mean value of the broken layers is 4.42738 with a variance of 1.2313. In the pulse factor data, the mean value of the complete layers is 4.3562 with a variance of 0.4341, and the mean value of the broken layers is 5.8589 with a variance of 2.1168. In the gravity frequency data, the mean value of the complete layers is 9.4144 with a variance of 0.0482, and the mean value of the broken layers is 9.3739 with a variance of 0.0557. In the gravity amplitude data, the mean value of the complete layers is 0.1535 with a variance of 0.0010, and the mean value of the broken layers is 0.1096 with a variance of 0.0016. In the effective values and the gravity amplitudes, the data are significantly larger in the complete layers than in the broken layers. In the kurtosis factors and the pulse factors, the data are significantly larger in the broken layers than in the complete layers. The gravity frequency is not significantly different in the complete and broken layers. Obviously, the calculation results are generally consistent with the analysis above. Among the five eigenvalues, the variances of the broken layers are greater than that of the complete layers. This is because there are some complete rock blocks in the broken layers, resulting in different conditions in each broken layer, which are reflected in significantly different vibration signals and more scattered eigenvalues.

After the above analysis, among the eigenvalues extracted from the vibration signal, the four eigenvalues of effective value, kurtosis factor, pulse factor, and gravity amplitude have obvious differences between the complete layers and the broken layers, which can be used as indicators to distinguish complete layers and broken layers.

4. Vibration Signal Processing Based on Wavelet Transform

4.1. Vibration Signal Denoising Based on Wavelet Transform. The wavelet transform threshold denoising method, a nonlinear denoising method first proposed by Johnstone and Donoho in 1992, can achieve approximate optimum in the sense of minimum mean square error with the simplest implementation and the least amount of computation. After wavelet decomposition, the amplitude of the wavelet coefficient of useful signals is generally large, while that of noises is small. It can be considered that the wavelet coefficient of useful signals is greater than that of noise signals. Wavelet threshold denoising is to find a reasonable threshold value as a distinction point that can distinguish the two coefficients. The wavelet coefficients of useful signals are larger than the threshold, and the wavelet coefficients of noise signals are smaller than the threshold. The wavelet coefficients of the noise signal are processed, and then, the wavelet coefficients of useful signals and the processed noise signals are restored to the original signal, which is the signal after denoising.

The signals measured by the instrument are

$$F(t) = s(t) + e(t). \tag{9}$$

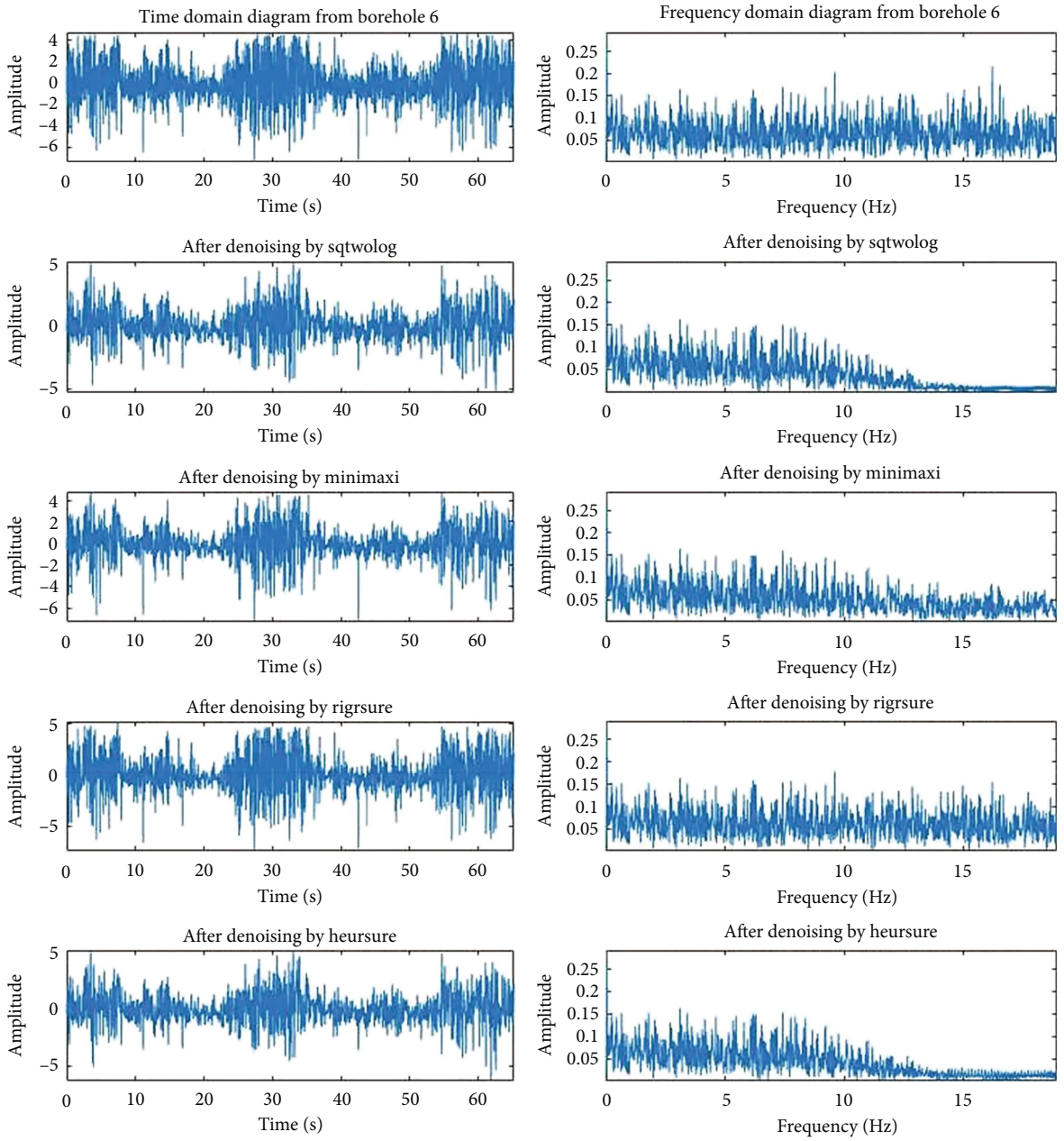

Figure 11: Denoising effect diagram of four threshold rules.

In the formula, $F(t)$ is the original signal, $s(t)$ is the useful signal, and $e(t)$ is the noise signal.

Both sides of Equation (9) are simultaneously wavelet transformed to obtain

$$\mathrm{WT}_f(a,b) = \mathrm{WT}_S(a,b) + \mathrm{WT}_e(a,b). \tag{10}$$

The wavelet transform of the measured signal is equal to the sum of multiple signal wavelet transforms.

For Equation (10), after the wavelet transform, most of the energy of the signal can be concentrated in the larger wavelet coefficients, while the amplitude of the wavelet coefficients of the noise signal is relatively small. The wavelet coefficients of the noisy signal are minimized and then used to reconstruct the signal for the purpose of denoising.

Wavelet threshold denoising of one-dimensional signal can be divided into three steps:

Table 1: Comparison of threshold denoising results.

Threshold rules	Energy ratio	SNR	Effective value
Sqtwolog	0.5330	3.3074	1.2452
Minimaxi	0.6625	4.7175	1.0586
Rigrsure	0.9029	10.1287	0.5678
Heursure	0.5416	3.3877	1.2337

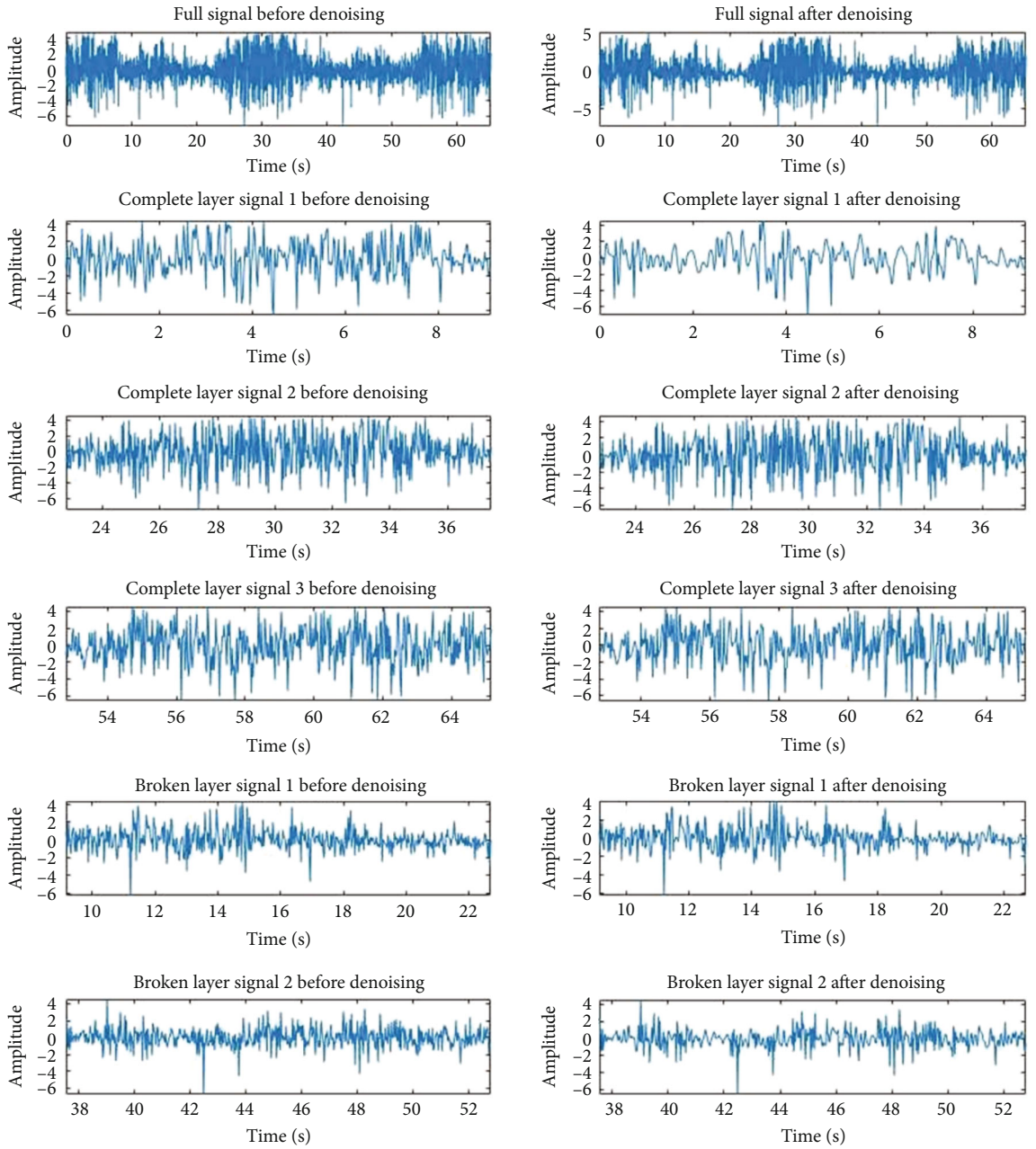

Figure 12: Denoising effect diagram of borehole 6 by rigrsure threshold rule.

(1) Select wavelet basis functions and decomposition layers, and perform wavelet decomposition on the signal

(2) Select a threshold value, and apply the threshold function to the obtained wavelet coefficients

(3) Reconstruct the thresholder wavelet coefficients to restore the original signal

In wavelet threshold denoising, the selection of threshold directly affects the denoising effect. There are four threshold selection methods for wavelet threshold denoising: general threshold rule (stqwolog), minimum maximum variance threshold (minimaxi), unbiased likelihood estimation rule (rigrsure), and heursure threshold rule (heursure).

Four threshold selection methods were applied to denoise the vibration signals obtained from borehole 6 separately, and one of the results with high signal-to-noise ratio should be selected for use. The time and frequency domain diagrams of the signals after denoising by applying the four threshold rules, respectively, are shown in Figure 11. The energy ratio, signal-to-noise ratio (SNR), and root mean square error (RMSE) of the signal after denoising for each threshold rule are found separately, as shown in Table 1.

From the comparison of the data in Table 1, it can be seen that after denoising by rigrsure, the energy ratio of

Table 2: Wavelet feature-scale entropy of borehole 6.

Layer	Subband 1	Subband 2	Subband 3	Subband 4	Subband 5	Subband 6	Subband 7	Subband 8
Complete layer 1	523.82	476.51	480.32	409.53	83.60	54.15	70.73	77.17
Complete layer 2	728.95	750.62	738.07	723.25	623.58	753.29	1008.63	1115.70
Complete layer 3	918.11	510.31	770.86	608.77	485.75	309.34	421.24	804.34
Broken layer 1	115.27	217.49	171.13	94.17	98.23	93.74	103.01	118.03
Broken layer 2	97.55	134.91	88.23	104.52	108.07	68.10	34.98	113.13

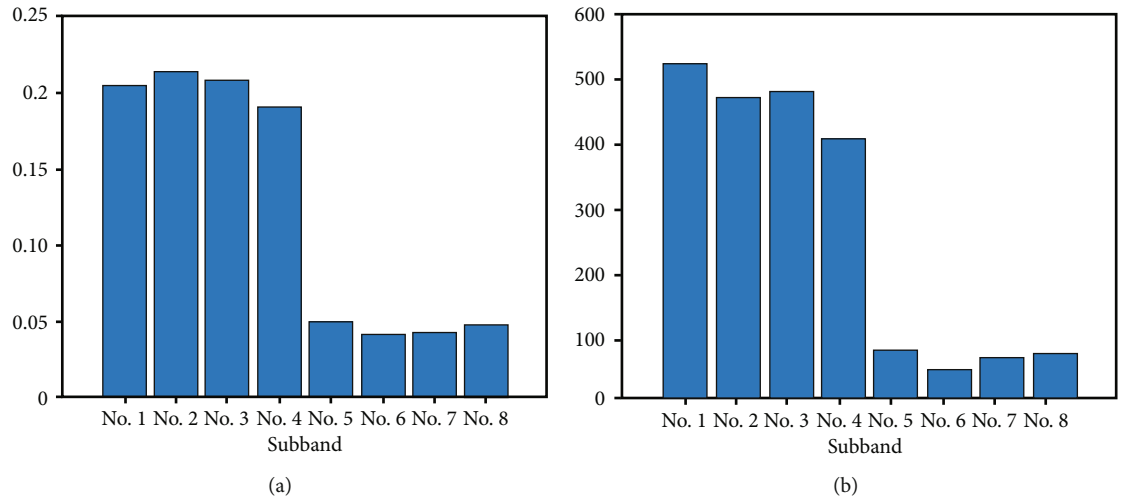

Figure 13: Wavelet decomposition subband energy ratio (a) and wavelet feature-scale entropy (b) of complete layer 1.

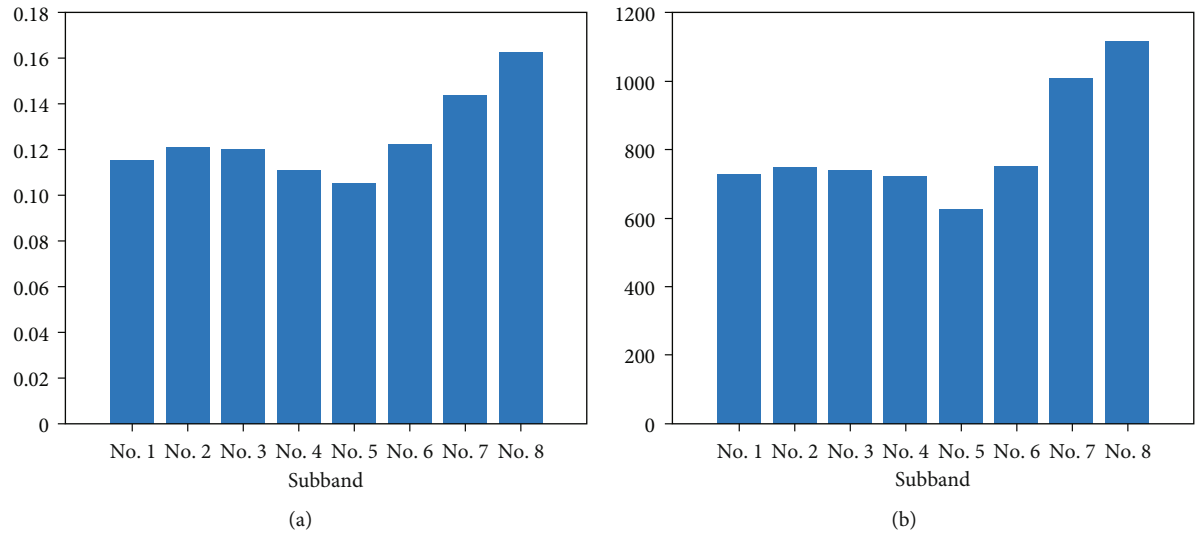

Figure 14: Wavelet decomposition subband energy ratio (a) and wavelet feature-scale entropy (b) of complete layer 2.

the denoised signal to the original signal is 0.9029, the signal-to-noise ratio is 10.1287, and the root mean square error is 0.5678. Among the four denoising threshold rules, its energy ratio and signal-to-noise ratio are the highest, and the root mean square error is the smallest, indicating that the signal after denoising by rigrsure can retain the characteristics of the original signal to the greatest extent. Therefore, in this paper, rigrsure is used for denoising vibration signals.

Taking borehole 6 as an example, its time domain diagrams before and after denoising are listed for comparison in Figure 12.

4.2. Extraction and Comparison of Wavelet Feature-Scale Entropy. The vibration signals were decomposed into three wavelet packets by db4 wavelet, obtaining 8 wavelet subbands. The ratio of energy to total energy and the wavelet feature-scale entropy value of each subband were calculated

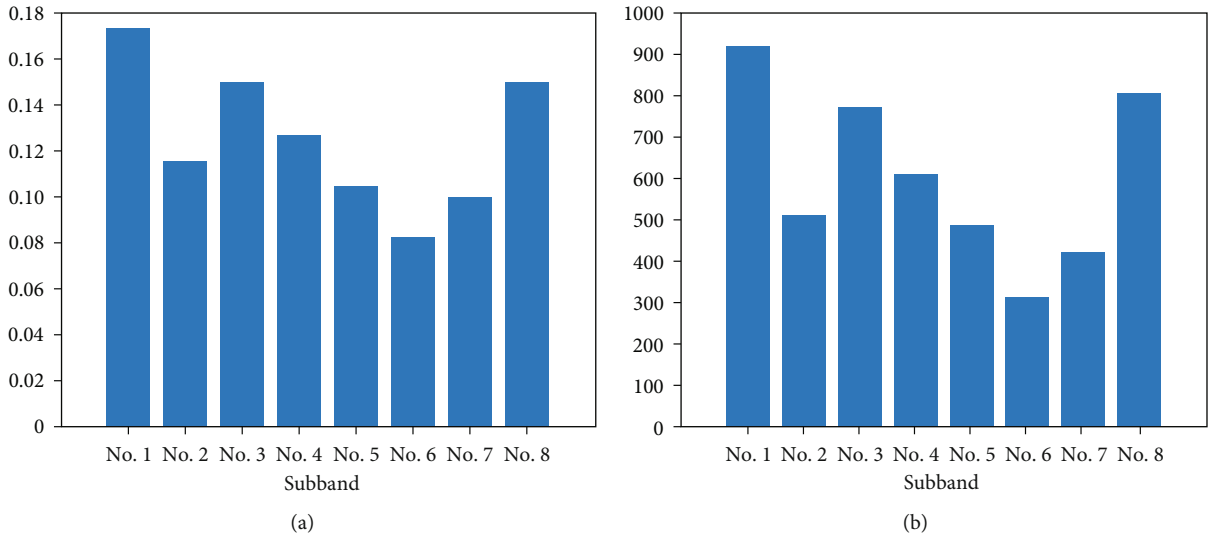

Figure 15: Wavelet decomposition subband energy ratio (a) and wavelet feature-scale entropy (b) of complete layer 3.

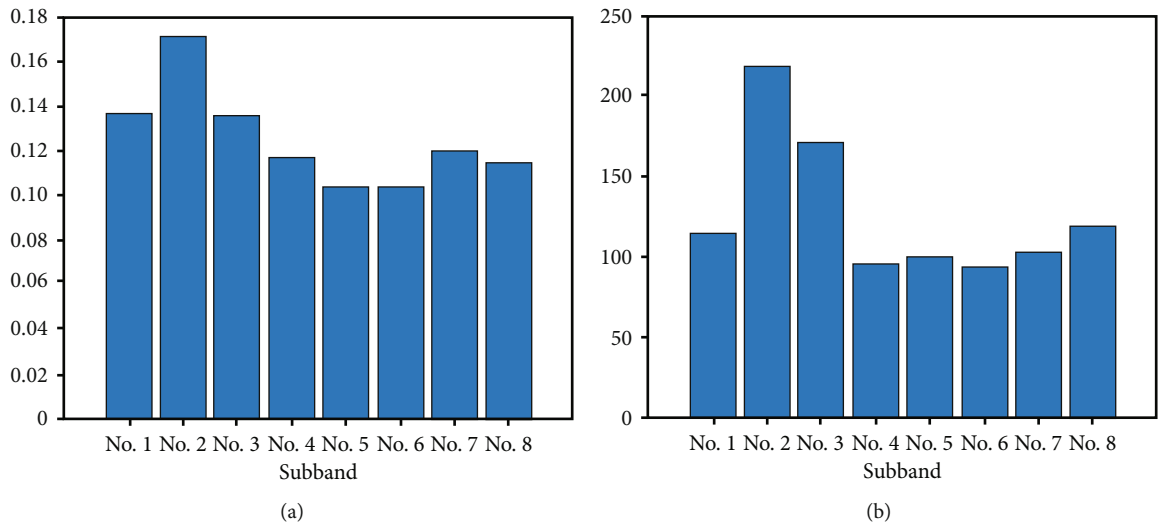

Figure 16: Wavelet decomposition subband energy ratio (a) and wavelet feature-scale entropy (b) of broken layer 1.

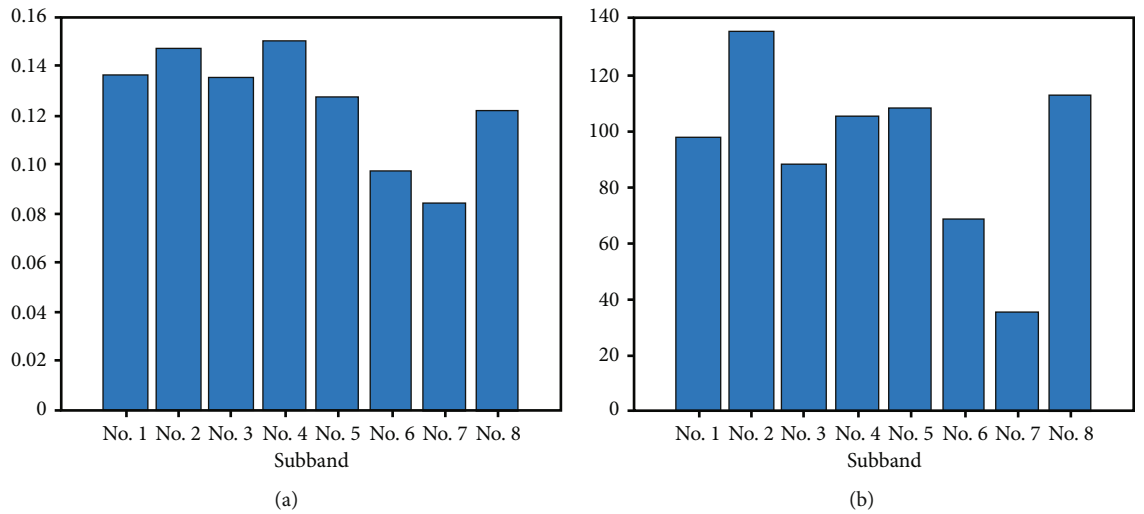

Figure 17: Wavelet decomposition subband energy ratio (a) and wavelet feature-scale entropy (b) of broken layer 2.

and plotted as a histogram, and the wavelet feature-scale entropy values are recorded in Table 2 to observe whether they were related to the integrity of rock layers.

The histograms of the wavelet subband energy ratios and the wavelet feature-scale entropy values for borehole 6 are listed in Figures 13–17 as an example.

As can be seen from the data in Table 2, the wavelet feature-scale entropy values for subband 1, for example, is 523.8267 for complete layer 1, 728.9507 for complete layer 2, 918.1105 for complete layer 3, 115.2788 for broken layer 1, and 97.5533 for broken layer 2. The results indicate that the wavelet feature-scale entropy values obtained by the db4 wavelet three-layer decomposition of the borehole 6 vibration signals are significantly larger in the first four subbands for the complete layers than for the broken layer. However, the values of the last four subbands of complete layer 1 differ greatly from the values of the first four subbands and are even smaller than the values of the broken layers, for reasons that may be related to the selected wavelet basis functions. The results of wavelet decomposition depend largely on the selection of wavelet basis functions, and the results vary when different wavelet basis functions are chosen for signal decomposition. Therefore, wavelet analysis can be used as a reference rather than a decisive factor to determine the complete and broken layers. In this part, more research is needed to determine the selection method of wavelet.

5. Conclusion

This paper focuses on the analysis and processing of drill pipe vibration signals, compares the analysis results of complete layers and broken layers by Fourier transform and wavelet transform, and finally obtains the eigenvalues of vibration signals. The conclusion mainly has the following 3 points:

(1) The drilling test was designed to simulate complete rock layers and broken rock layers of roadway roofs by superimposing complete specimens and broken specimens on each other, and the drill pipe vibration signals were obtained by the drilling test

(2) The results of the time and frequency domain analysis for vibration signals based on Fourier transform showed that the effective value, kurtosis factor, pulse factor, and gravity amplitude were sensitive to rock integrity, which could be used as indicators to identify whether the rock formation is intact

(3) The wavelet threshold denoising can be used to adaptively reduce the noise of signals, and the unbiased likelihood estimation threshold rule had the best denoising effect among the four threshold rules, so that the useful information can be retained to the maximum extent after denoising

Data Availability

The data that support the findings of this study are available from the corresponding author upon reasonable request.

Conflicts of Interest

The authors declare that they have no conflicts of interest.

References

[1] M. Qin, K. Wang, K. Pan, T. X. Sun, Z. Liu, and Z. G. Liu, "Analysis of signal characteristics from rock drilling based on vibration and acoustic sensor approaches," *Applied Acoustics*, vol. 140, pp. 275–282, 2018.

[2] P. Flegner, J. Kačur, M. Durdán, I. Leššo, and M. Laciak, "Measurement and processing of vibro-acoustic signal from the process of rock disintegration by rotary drilling," *Measurement*, vol. 56, pp. 178–193, 2014.

[3] P. Flegner, J. Kačur, M. Durdán, and M. Laciak, "Processing a measured vibroacoustic signal for rock type recognition in rotary drilling technology," *Measurement*, vol. 134, pp. 451–467, 2019.

[4] K. L. Johnson, *Contact Mechanics*, Combridge University Press, Combridge, 2012.

[5] T. D. Cheng, Z. Z. Zhang, Q. W. Yi, B. Y. Yi, and H. P. Yuan, "Denoising method of rock acoustic emission signal based on improved VMD," *Journal of Mining and Strata Control Engineering*, vol. 4, pp. 1–10, 2022.

[6] Y. C. Li, Y. D. Qu, Q. Y. He, and C. N. Tang, "Mesoscale numerical study on the evolution of borehole breakout in heterogeneous rocks," *International Journal for Numerical and Analytical Methods in Geomechanics*, vol. 44, no. 8, pp. 1219–1236, 2020.

[7] P. A. Lindqvist, H. L. Lai, and O. Alm, "Indentation fracture development in rock continuously observed with a scanning electron microscope," *International Journal of Rock Mechanics and Mining Sciences & Geomechanics Abstracts*, vol. 21, no. 4, pp. 165–182, 1984.

[8] S. F. Liu, P. Shi, Z. J. Wan, J. K. Lv, S. F. Lu, and Y. C. Wang, "Study on influence laws of strata behaviors for shallow coal seam mining beneath gully terrain," *Journal of Mining and Strata Control Engineering*, vol. 2021, article 3954659, 12 pages, 2021.

[9] X. L. Liu, Z. Liu, X. B. Li, F. Q. Gong, and K. Du, "Experimental study on the effect of strain rate on rock acoustic emission characteristics," *International Journal of Rock Mechanics and Mining Sciences*, vol. 133, article 104420, 2020.

[10] Y. X. Liu, M. S. Gao, H. S. Zhao, S. L. He, Z. G. Li, and Z. Z. Cong, "Detection of overlying rock structure and identification of key stratum by drilling and logging technology," *Journal of Mining and Strata Control Engineering*, vol. 2, pp. 1–8, 2020.

[11] T. Andrzej, P. Zenon, S. Krzysztof, W. Rafal, K. Krzysztof, and S. Stanislaw, "Assessment of ground vibrations indi ced by gas and oil well drilling using numerical, simulations," *Archives of Mining Sciences*, vol. 64, pp. 1–12, 2019.

[12] Y. P. Li, F. Cui, W. H. Yang, and X. Q. Yuchi, "Dynamic migration law and its control of roof in fully mechanized top coal caving mining in extremely steep and thick coal seams," *Journal of Mining and Strata Control Engineering*, vol. 2, article 043538, 2020.

[13] Y. Xue, J. Liu, P. G. Ranjith, F. Gao, H. Xie, and J. Wang, "Changes in microstructure and mechanical properties of low-permeability coal induced by pulsating nitrogen fatigue fracturing tests," *Rock Mechanics and Rock Engineering*, pp. 1–20, 2022.

[14] Y. Xue, P. G. Ranjith, Y. Chen, C. Cai, F. Gao, and X. Liu, "Nonlinear mechanical characteristics and damage constitutive model of coal under CO_2 adsorption during geological sequestration," *Fuel*, vol. 331, article 125690, 2023.

[15] Z. L. Yan, F. Dai, Y. Liu, and H. B. Du, "Experimental investigations of the dynamic mechanical properties and fracturing behavior of cracked rocks under dynamic loading," *Bulletin of Engineering Geology and the Environment*, vol. 79, no. 10, pp. 5535–5552, 2020.

[16] H. P. Kang, G. Xu, B. M. Wang et al., "Forty years development and prospects of underground coal mining and strata control technologies in China," *Journal of Mining and Strata Control Engineering*, vol. 1, article 013501, 2019.

[17] N. K. Krishnan and K. Anne, "Derivation of a damage sensitive feature using the Haar wavelet transform," *Journal of Ap-plied Mechanics*, vol. 76, no. 6, pp. 1–14, 2009.

[18] G. F. Wang, Y. H. Pang, and H. E. Ren, "Intelligent coal mining pattern and technological path," *Journal of Mining and Strata Control Engineering*, vol. 2, article 013501, 2020.

[19] E. Zhao, K. Li, X. Yang, and N. Deng, "Speculum observation and trajectory measurement in gas extraction drilling: a case study of Changling coal mine," *Geofluids*, vol. 2021, Article ID 5545067, 16 pages, 2021.

[20] X. Zhang, H. Wang, D. Zhao et al., "New insights into the drill cutting characteristics and fault distribution in gas-containing coal seams," *Geofluids*, vol. 2022, Article ID 3201581, 14 pages, 2022.

[21] Y. Gao, Y. Zhang, Z. Zhang et al., "Parametric study of the borehole drilling in jointed rock mass," *Geofluids*, vol. 2021, Article ID 8237199, 14 pages, 2021.

[22] O. Su, "Performance evaluation of button bits in coal measure rocks by using multiple regression analyses," *Rock Mechanics and Rock Engineering*, vol. 49, no. 2, pp. 541–553, 2016.

[23] D. Zhang, N. Zhao, M. Tong, and C. Du, "Design of the rock coal shearer cutting mechanism and its vibration analysis," in *2016 IEEE International Conference on Mechatronics and Automation*, pp. 720–725, Harbin, China, 2016.

[24] X. Cao, X. Li, F. Yue, and H. Sun, "Research and application of vibration measurement while drilling in the undersea coal mine," *Journal of Coastal Research*, vol. 103, pp. 323–327, 2020.

[25] W. Zhang, C. Li, J. Jin, X. Qu, S. Fan, and C. xin, "A new monitoring-while-drilling method of large diameter drilling in underground coal mine and their application," *Measurement*, vol. 173, article 108840, 2021.

[26] B. Li, Z. Li, E. Wang et al., "Discrimination of different AE and EMR signals during excavation of coal roadway based on wavelet transform," *Minerals*, vol. 12, no. 1, p. 63, 2022.

[27] M. Zolgharni, B. J. Jones, R. Bulpett, A. W. Anson, and J. Franks, "Energy efficiency improvements in dry drilling with optimised diamond-like carbon coatings," *Diamond & Related Materials*, vol. 17, pp. 1733–1737, 2007.

[28] Y. L. Zhao, Y. X. Wang, W. Wang, L. Tang, Q. Liu, and G. Cheng, "Modeling of rheological fracture behavior of rock cracks subjected to hydraulic pressure and far field stresses," *Theoretical and Applied Fracture Mechanics*, vol. 101, pp. 59–66, 2019.

[29] B. Gui, C. H. Li, T. J. Liu, J. H. Wang, Y. L. Zheng, and S. Y. Gong, "Research on advanced detection technology of roadway excavation based on vibration wave CTinversion," *Journal of Mining and Strata Control Engineering*, vol. 3, pp. 1–6, 2021.

[30] Y. L. Zhao, L. Y. Zhang, W. J. Wang, Q. Liu, L. M. Tang, and G. Cheng, "Experimental study on shear behavior and a revised shear strength model for infilled rock joints," *International Journal of Geomechanics*, vol. 20, no. 9, pp. 1–12, 2020.

[31] Y. L. Zhao, L. Y. Zhang, J. Liao, W. J. Wang, Q. Liu, and L. Tang, "Experimental study of fracture toughness and subcritical crack growth of three rocks under different environments," *International Journal of Geomechanics*, vol. 20, no. 8, pp. 1–11, 2020.

[32] Y. J. Guo, F. Luo, M. Li, G. Sun, Y. L. Diao, and P. D. Xu, "Development and evolution of tension-shear failure network of surrounding rock in square roadway," *Journal of Mining and Strata Control Engineering*, vol. 4, pp. 1–9, 2022.

[33] J. Wang and X. L. Wang, "Seepage characteristic and fracture development of protected seam caused by mining protecting strata," *Journal of Mining and Strata Control Engineering*, vol. 3, pp. 1–7, 2021.